Physics and chemistry of interstellar ice

Guss, K.M.R.

Chapter VI

LASER DESORPTION TIME-OF-FLIGHT MASS SPECTROMETRY OF CRYOGENIC ICES

Laser desorption time-of-flight mass spectrometry of cryogenic ices
K. Isokoski, J.-B. Bossa, D. M. Paardekooper, and H. Linnartz
Reviews of Scientific Instruments, 2013, to be submitted.

Abstract

Our current understanding of complex solid state astrochemical processes in interstellar ices is limited by the available experimental techniques. The abundance of species decreases with increasing size and complexity, making sensitivity of the analysis methods crucial for characterizing processes leading to prebiotic molecules, while simultaneously maintaining the conditions relevant to the interstellar medium. In this paper we introduce a new sensitive technique for the controlled formation of complex molecules in interstellar ice analogs, with minimal chemical alteration as the primary objective. The experiment uses UV laser desorption combined with time-of-flight mass spectrometry, providing a tool for *in situ* and real-time analysis. The technique is demonstrated for astronomically relevant ice components: methanol (CH_3OH), methyl formate ($HCOOCH_3$) and ethane (C_2H_6). We show that UV photo-processing of solid C_2H_6 ice yields species with possibly up to 6 carbon atoms, most likely in cyclic unsaturated structures.

6.1 Introduction

Formation of complex organic interstellar molecules[1] is subject to intensive research due to its relevance to the origin of life. The presence of prebiotic species, such as aminoacids, in meteoritic samples (Kvenvolden et al. 1970, Cronin & Pizzarello 1997, Lawless et al. 1972, Ehrenfreund et al. 2001) suggests an exogenous formation mechanism (Botta & Bada 2002, Sephton 2002). As is the case for other solar system bodies, meteorites have their origin in icy dust grains, which act as important chemical catalysts in the sparse interstellar medium (ISM). In the cold (<100 K) protostellar phase the ice comprises a rich mixture of species accreted and formed on the grain surface (Tielens & Hagen 1982) which later become incorporated in meteorites and/or cometary material. Remote observations of interstellar ices are limited to major ice components with abundances $\gtrsim$1 % with respect to H_2O (*e.g.*, CO, CO_2, CH_3OH, CH_4, NH_3) (Whittet et al. 1996, Gibb et al. 2004, Boogert et al. 2008, Pontoppidan et al. 2008, Bottinelli et al. 2010). However, after the thermal desorption of ice mantles (>100 K), several complex molecules are detected in the gas phase, particularly in hot molecular cores of protostars (Herbst & van Dishoeck 2009). Many of the observed complex molecules are likely to form in the solid state before ice mantle evaporation (Garrod & Herbst 2006, Garrod et al. 2008, Öberg et al. 2009b).

Experimental solid-state astrochemistry provides a way to study interstellar chemical reactions under controlled laboratory conditions and to identify the steps required for the formation of complex molecules. Formation of interstellar methanol (CH_3OH) has been shown to proceed through successive hydrogenation of CO ice (Hiraoka et al. 2002, Watanabe & Kouchi 2002, Fuchs et al. 2009). From CH_3OH, larger and more complex species, such as dimethylether (CH_3OCH_3) and glycolaldehyde ($HOCH_2CHO$), can form by UV photolysis and thermal radical-radical/radical-neutral recombinations (Öberg et al. 2009b). Despite their likely solid-state origin, these species have been detected in the ISM only in the gas phase (Snyder et al. 1974, Winnewisser & Gardner 1976, Hollis et al. 2000, Beltrán et al. 2009). In the laboratory, energetic processing of interstellar ice analogs comprising of species commonly observed in real interstellar ices results in rich mixtures of complex molecules including amino-acids (Hagen et al. 1979, Schutte et al. 1993b, Bernstein et al. 1995, Greenberg et al. 2000, Bernstein et al. 2002, Muñoz Caro et al. 2002, Muñoz Caro & Schutte 2003,

[1] Complex organic interstellar molecules = carbon-containing species with ≥6 atoms

Elsila et al. 2007, Nuevo et al. 2008, 2010), yet to be observed in the ISM. The outcome of these initial experiments has however been questioned, as the analysis has not been done for samples *in situ*, under conditions relevant to the interstellar medium.

The analysis of non-volatile organic residue (including amino-acids) is typically done by Gas Chromatography-Mass Spectrometry (GC-MS) and Liquid Chromatography-Mass Spectrometry (LC-MS). GC and LC require thermal and chemical alteration of the sample, which is likely to change its composition. Temperature Programmed Desorption (TPD), commonly used for the analysis of more volatile ice components, also allows thermal reactions prior to the analysis. Although sensitive, these analysis techniques are thus inherently prone to uncertainty. Fourier Transform InfraRed (FTIR) spectroscopy enables remote analysis of the sample composition without chemical alteration. Due to spectral overlap of different absorption features however, IR spectroscopy of ice analogs has a detection limit of ~1 % making it unsuitable for detailed analysis of complex ice mixtures, where spectral overlap will cause ambiguity.

Laser desorption is a powerful alternative to bring non-volatile and/or thermally unstable molecules into the gas phase, and is widely used in mass-spectrometric sample characterization (Levis 1994, Posthumus et al. 1978, Hahn et al. 1988, Karas et al. 1987). For interstellar ice analogues, the main advantage is that the method allows sampling at any temperature below sublimation. This technique has been recently demonstrated for polycyclic aromatic hydrocarbons in interstellar ice analogs (Gudipati & Yang 2012). Combined with Time-Of-Flight Mass Spectrometry (TOF-MS) (Guilhaus 1995). a complete mass spectrum can be recorded for each desorption pulse at a high repetition rate. Here we describe a new experiment, Mass-Analytical Tool for Reactions in Interstellar ICES (MATRI^{2}CES), where pulsed laser desorption is applied to the analysis of astronomically relevant cryogenic (17-100 K) ice samples.

6.2 Instrumentation

Fig. 6.1 shows a schematic overview of the experimental setup. The setup is composed of (i) a main UHV chamber, (ii) an ionization chamber, and (iii) a TOF chamber (flight tube). The main chamber is where cryogenic samples are grown, processed and injected into the carrier gas by laser desorption. Carrier gas admitted from a pulsed valve transports the desorbates into the ionization chamber through two collimating skimmers. The desorbates are ionized by electron impact and accelerated into the TOF chamber for mass analysis.

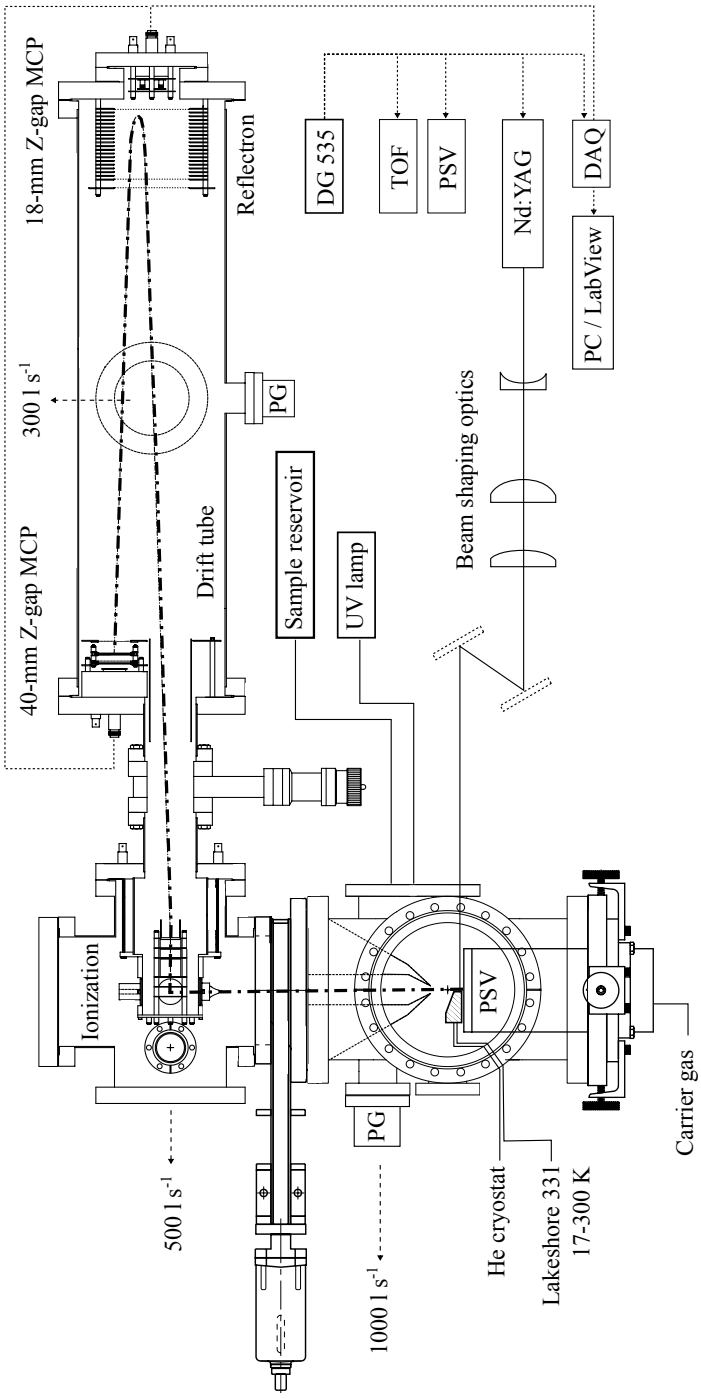

Figure 6.1 – Schematic diagram of MATRI^{2}CES.

MATRI^{2}CES is an Ultra-High Vacuum (UHV) experiment with a base pressure of $\sim 10^{-10}$ mbar. The main, ionization and TOF chambers are evacuated by turbomolecular pumps (Varian TV1001, TV551 and TV301 Navigator) at pumping speeds of ~1000, 500 and 300 l s^{-1}, respectively. The turbomolecular pumps are backed by oil-free foreline dry scroll pumps (Varian TS300 for TV1001 and TS600 for both TV551 and TV301). Working pressures from main to TOF chamber are $\sim 10^{-6}$, 10^{-8} and 10^{-9} mbar. Details of the experiment and measuring procedure are given below.

6.2.1 Substrate

The sample substrate is located in the center of the main chamber. The substrate is a uniform gold-coated copper block with a 2 × 50 mm (or 15 × 50 mm) rectangular sampling area and a 20° knife edge to minimize disruption of the carrier flow (see Fig. 6.2). The substrate is connected to a closed-cycle helium cryostat (Advanced Research Systems, DE 202), which has a cooling capacity enabling temperatures as low as 17 K. Substrate temperature is controlled between 17 and 300 K by a temperature controller (LakeShore 331) with a resistive heater element and a chromel-gold/iron thermocouple mounted on the base of the substrate. To cover the 50-mm long sampling area, the cryostat is situated on top of a bellow with a motorized linear shift mechanism with an adjustable translation speed (UHV design, LSM64-50, McLennan, 23HT18C stepper motor with a SimStep single axis stepper system).

6.2.2 Sample deposition

Samples are grown onto the cold substrate by vapor deposition from an external gas reservoir. Gases are admitted into the vacuum chamber via a precision leak valve (Hositrad) with a metal capillary directed onto the substrate at a distance of ~2.5 cm. During deposition the substrate is translated vertically to obtain a uniform ice distribution across the sampling surface.

6.2.3 Processing

To trigger astronomically relevant chemical reactions, the deposited samples are exposed to vacuum UV irradiation from a microwave stimulated hydrogen flow discharge lamp, separated from the vacuum chamber by a MgF_2 window. The emission spectrum of the lamp peaks around Ly-α at 121.6 nm with coverage over 115-170 nm (7-10.5 eV) (Muñoz Caro & Schutte 2003). The photon flux of the lamp is estimated to be $\sim 5 \times 10^{13}$ s^{-1} cm^{-2} (Öberg et al. 2007). The emission of the lamp largely resembles the UV radiation field deep inside interstellar clouds (Kim et al. 1994, Muñoz Caro & Schutte 2003). In dense clouds, cosmic rays lead to the internal production of UV photons through secondary electron excitation of H_2 (Prasad & Tarafdar 1983, Gredel et al. 1989).

6.2.4 Laser desorption

Desorption of processed ice is induced by a 3-4-ns laser pulse from a 355-nm Nd:YAG laser (Polaris II, New Wave Research). The laser is operated at a repetition rate of 10 Hz and an adjustable pulse energy of 3-8 mJ. The beam diameter (2.5 mm) is reduced using a Galilean beam expander assembly

consisting of a plano-concave ($f = -2.5$ mm) and a plano-convex lens ($f = +25$ mm) resulting in a collimated 25-mm diameter beam. The expanded beam is subsequently focused onto the substrate by a cylindrical lens ($f = +750$ mm) producing a thin uniform intensity line focus across the entire substrate. The beam waist, w_F, is given by Eq. 6.1

$$w_F = \frac{\lambda f M^2}{\pi w_L} \tag{6.1}$$

where λ = laser wavelength, f = focal length of the focusing lens and w_L = radius of the collimated beam at the lens. M^2 is the laser beam quality factor (19.4). The resulting vertical thickness of the laser line, $2w_F$, is 0.09 mm. Two laser mirrors are used to align the laser focus onto the substrate. All components are anti reflection coated UV fused silica (SiO_2). The reflectivity of the optical components and the entry port to the vacuum chamber decreases the initial pulse energy by about 7 %.

6.2.5 Entrainment

A pulsed supersonic valve (PSV) (Jordan TOF Products, Inc.) is used to generate an intense short gas pulse, which carries the desorbed molecules from the ice surface to the ionization chamber. We use He as carrier gas to avoid condensation of carrier onto the cold substrate. The valve employs a magnetic beam repulsion principle in a current loop mechanism (Dimov 1968, Gentry & Giese 1978, Byer & Duncan 1981, Rorden & Lubman 1983). A 20-μs 4.2-kA current pulse passes through two parallel beam conductors in a hairpin configuration (Fig. 6.2). The consequent magnetic force lifts the top beam allowing gas to pass through the o-ring seal. The He gas (backing pressure ~7 bar) is thereby admitted to the 0.5-mm nozzle creating a ~60 μs expansion into the vacuum.

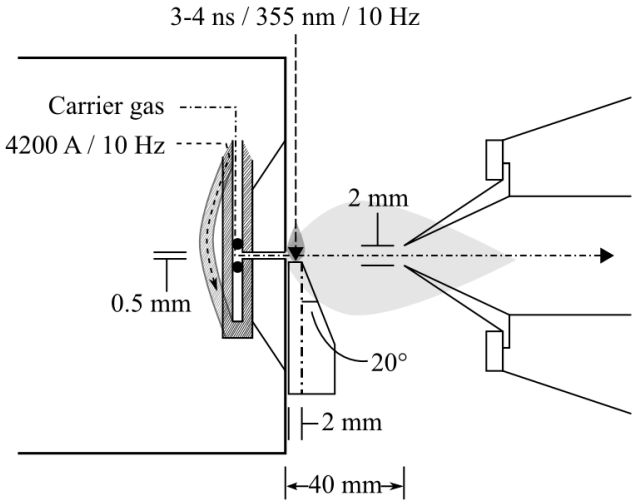

Figure 6.2 – Schematic drawing of the sampling area. PSV valve is depicted in the left, substrate immediately in front of it and front skimmer on the right.

The substrate is placed as close as possible to the valve body to minimize the disturbance to the gas expansion. A gap of ~1 mm is left to avoid thermal contact between the cooled substrate and the valve body. The substrate is mounted on an additional translator to adjust the distance to the gas expansion axis, which influences the entrainment of desorbates (Boogaarts 1996).

Sample molecules injected into the gas expansion are instantaneously cooled through multiple collisions with He atoms. The most efficient energy transfer occurs at the highest density region close to the nozzle, resulting in rotational temperatures as low as 5 K (Meijer et al. 1990).

The entrainment in supersonic gas allows fast transport (about 1800 m s^{-1}) of the desorbed molecules to the ionization region. Furthermore, in a supersonic beam, molecules travel at a narrow Maxwellian velocity distribution strongly peaking at the average velocity (Smalley et al. 1977). This prevents additional spatial spreading of molecules injected into the expansion. Fast collisional cooling of the desorbed molecules also minimizes chemical reactions during the transport. Before entering the ionization region, the resulting molecular expansion is collimated by two skimmers with orifices of 2 and 1 mm, situated at 4 and 31 cm from the nozzle orifice.

6.2.6 Time-of-flight mass analysis

The desorbates are analyzed mass spectrometrically in a custom-built Wiley-McLaren type orthogonal acceleration reflection time-of-flight mass spectrometer (ReTOF-MS, Jordan TOF Products, Inc.). The desorbates and He are ionized through electron impact (EI, see Sect. 6.2.7). Electrons are ejected from a hot wire filament and accelerated to 70 eV. At this energy the de Broglie wavelength matches the typical bond length in organic molecules giving a maximum ionization efficiency. The ions are generated between a repeller plate and an extraction grid, which for the duration of ionization (10 μs) are at equal potential (1500 V). After ionization, the grid voltage is lowered by 200 V, which extracts the generated cations to the next section. The cations are accelerated by an acceleration grid at ground potential. The accelerated ion beam crosses a focusing *Einsel lens* and deflection plates (60 V) before entering the field free drift (flight) tube.

Cations and radical cations with different m/z ratio separate in the drift tube (81 cm) according to the acquired velocities. The spectrometer can be operated in linear or reflection mode. In linear mode, the ions pass the grounded reflector assembly and are collected at a MCP (microchannel plate) detector (18 mm). In reflection mode, an assembly of retarder grid (+700 V) and reflector grid (+1200 V) mirrors the ions back into the field-free drift tube to be collected at a secondary MCP detector (40 mm). The detectors are high-sensitivity triple (Z-gap) MCP detectors with a $10^9 - 10^{11}$ fold gain and a sub-nanosecond rise time. The reflector increases the flight distance from ~115 to ~195 cm.

6.2.7 EI Ionization

EI ionization produces predominantly a singly charged radical cation (Eq. 6.2)

$$M + e^- \rightarrow M^{+\bullet} + 2e^- \tag{6.2}$$

where M is the neutral analyte and $M^{+\bullet}$ is the radical cation. Molecular fragmentation (Eqs. 6.3 and 6.4) is common in EI sources which complicates the identification of the parent neutral, but can

also give information about its molecular structure.

$$M_1^{+\bullet} \rightarrow M_2^{+\bullet} + M_n \tag{6.3}$$

$$M_1^{+\bullet} \rightarrow M_2^{+} + M_n^{\bullet} \tag{6.4}$$

where $M_1^{+\bullet}$ is the parent radical cation, $M_2^{+\bullet}$ is a radical cation fragment, M_2^{+} is a cation fragment and $M_n^{(\bullet)}$ is a neutral radical fragment.

6.3 Results

6.3.1 Calibration

The TOF mass spectrometer is calibrated using a noble gas mixture (He 88 %; Ar 4 %; Kr 4 %; Xe 4 %; Linde gas). Fig. 6.3 shows a TOF mass spectrum of the gas mixture as pulsed from the PSV. We employ a conventional TOF equation:

$$\mathrm{TOF} = A + B \times \sqrt{m/z} \tag{6.5}$$

for 2-point calibration (Håkansson et al. 1998). To find parameters A and B we set $^4He^+$ at 4.00260 amu and $^{132}Xe^+$ at 131.90414 amu, while the other components and their isotopes are used to test the accuracy of the calibration. The resulting mass accuracy is better than 200 ppm for the used mass range.

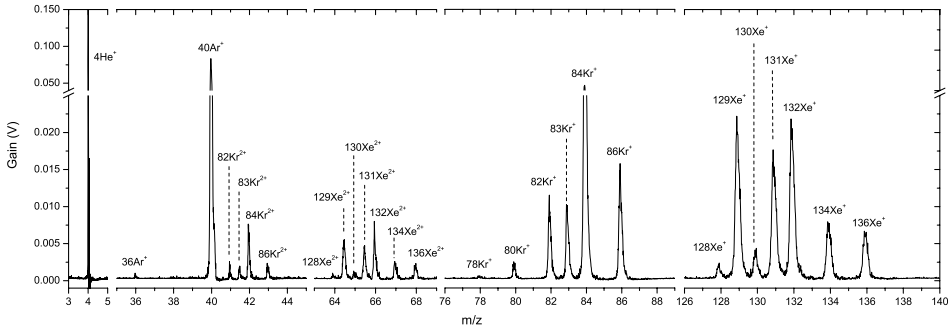

Figure 6.3 – TOF mass spectrum of the calibration gas mixture.

6.3.2 Carrier gas profile

In order to locate and characterize the profile of the He expansion, the MCP gain is monitored as a function of ion extraction time for m/z = 4 (He). Ion extraction before the arrival of He into the ionization zone leads to zero gain. Extraction during the transient He pulse leads to gain that

depends on the concentration of He atoms in the ionization region. Plotting the gain vs. extraction time thus gives the density profile of He in the gas expansion.

Fig. 6.4 shows the density profile of He in a pure gas expansion for different substrate positions. The different positions correspond to distance between the substrate surface and the expansion axis. The different results are a consequence of the actual configuration in which the substrate may entirely block or at least degrade the He flow. Almost no He is transmitted within a distance of ±0.5 mm from the expansion axis. Between 0.5 and 3 mm the transmission gradually increases. The density profile gradually sharpens and shifts towards lower extraction time. At 2 mm the front of the He profile is indistinguishable from those at and beyond 3 mm. However, the rear of the profile is degraded. At substrate distances of 3 mm and beyond, the He profile does not change indicating that the substrate no longer disturbs the expansion. Table 6.1 shows the peak delay and FWHM of the He profile for different substrate positions.

For further experiments, we adopt a distance of 1 mm. Here the substrate is close to the expansion axis ensuring efficient entrainment of desorbates, while leaving the He expansion relatively structured. No significant difference in He profile is observed for substrates with different width.

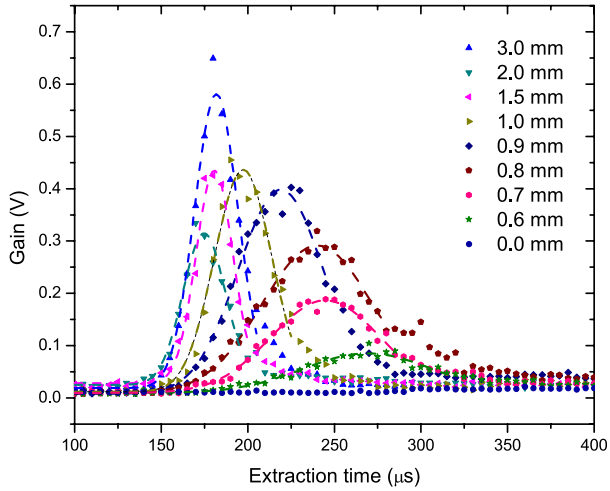

Figure 6.4 – He density profiles at different substrate positions, derived from the maximum intensity of m/z 4 as a function of extraction time. Position 0 mm corresponds to a configuration where the substrate surface coincides with the expansion axis. The dashed lines are Gaussian fits to the datasets, excluding tail structures characteristic to all positions.

6.3.3 Laser desorption of pure ices

In order to test the laser desorption of cryogenic samples, ices composed of different astronomically relevant molecules are used; methyl formate ($HCOOCH_3$), ethane (C_2H_6) and methanol (CH_3OH). Ice samples are grown by directed vapor deposition on a 15 mm wide substrate at 17 K. Typical

Table 6.1 – Influence of the substrate on the density profile of the carrier gas pulse. Peak delay (relative to the undisturbed flow; in μs), FWHM (μs) and integrated area (V μs) for the He profiles are derived from Gaussian fits to the data sets shown in Fig. 6.4. The setting marked in bold is used for further experiments.

Distance (mm)	Delay (μs)	FWHM (μs)	Area (V μs)
0.6	88	75	7.1
0.7	63	63	13.9
0.8	58	64	22.5
0.9	38	48	22.2
1.0	**16**	**33**	**17.7**
1.5	-1	21	10.9
2.0	-7	25	9.0
3.0	0	25	17.8
4.0	-0	25	17.7
5.0	0	25	17.8

deposition time is ~15 min, during which ices of several thousands of monolayers thick ($\gg$1 μm) are grown. Ices are laser desorbed at 17 K at a pulse energy of ~7 mJ and thereby injected into the He expansion. Ionization/extraction is carried out at an extraction time coincident with the peak intensity of the He profile. Fig. 6.5 shows the TOF mass spectra for laser-desorbed $HCOOCH_3$, C_2H_6 and CH_3OH ice.

EI ionization of $HCOOCH_3$ proceeds through generation of the parent radical cation $HCOOCH_3{}^{+\bullet}$, followed by fragmentation:

$$\begin{aligned} HCOOCH_3^{+\bullet} + e^- &\rightarrow OCH^+ + OCH_3^\bullet \\ &\rightarrow OCH^\bullet + OCH_3^+ \\ &\rightarrow CH_3^+ + HCO_2^\bullet \\ &\rightarrow CH_3^\bullet + HCO_2^+ \,(\rightarrow CO_2^{+\bullet}) \end{aligned}$$

C_2H_6 produces a parent radical cation $C_2H_6{}^{+\bullet}$ followed by fragmentation with most intense signal from $C_2H_4{}^{+\bullet}$. CH_3OH yields radical cation $CH_3OH^{+\bullet}$, which fragments through:

$$\begin{aligned} CH_3OH^{+\bullet} + e^- &\rightarrow OCH_3^+ + H^\bullet \\ &\rightarrow CH_2O^{+\bullet} + H_2 \rightarrow OCH^+ \\ &\rightarrow CH_3^+ + OH^\bullet \end{aligned}$$

TOF mass spectra of laser-desorbed $HCOOCH_3$, C_2H_6 and CH_3OH ice agree with the 70-eV electron ionization fragmentation pattern reported for these molecules in the NIST Chemistry Webbook (webbook.nist.gov/chemistry/). The similarity of the fragmentation pattern indicates that for the ices in question, the laser desorption process, as far as we are able to discriminate, does not chemically alter the sample. Indeed, the photon energy of the desorption laser (3.5 eV) is below the typical bond dissociation energy in organic molecules, and dissociation is therefore not expected

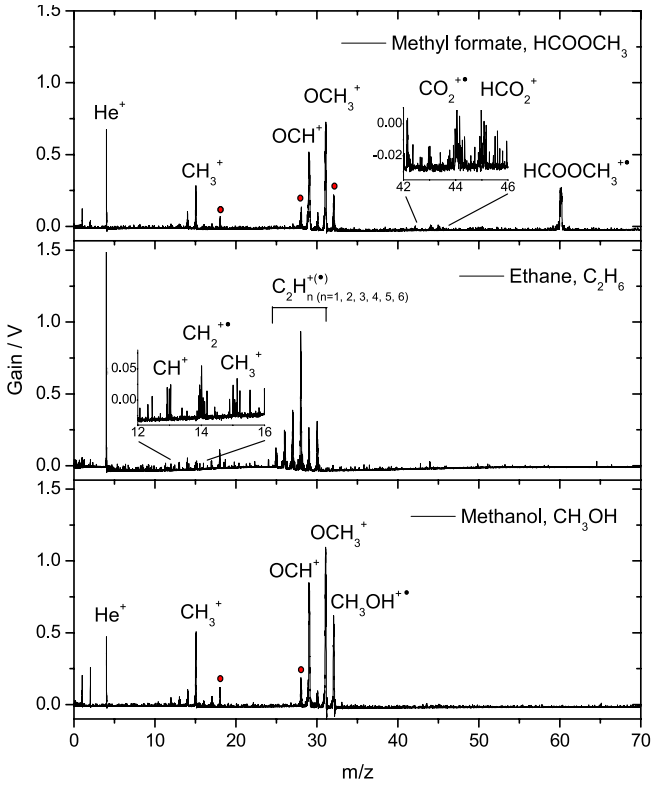

Figure 6.5 – Laser desorption (reflection) TOF mass spectra of pure $HCOOCH_3$, C_3H_6 and CH_3OH ice at 17 K. The most prominent mass fragments are labeled. The masses marked with a red dot correspond to residual atmospheric gases H_2O, N_2 and O_2.

to occur. However, a soft ionization technique (*e.g.*, single-photon ionization, SPI) will be beneficial in avoiding the fragmentation after ionization and thus in confirming the delicateness of the desorption process itself.

UV laser desorption is a suitable evaporation method for astronomical ices as demonstrated for pure $HCOOCH_3$, C_2H_6 and CH_3OH ices. The UV desorption proceeds through coupling of the laser energy to the substrate, inducing fast local desorption of the cryogenic sample. For matrix-assisted laser desorption of biomolecules, a wavelength close to the absorption frequency of the matrix is used. For interstellar ice analogues rich in water, wavelengths resonant with H_2O (IR) may be more efficient for consistent desorption. Targeted desorption may also enable layer-by-layer desorption and hence depth profiling of samples. The composition of processed interstellar ice analogs is likely to be inhomogenous due to the limited penetration depth of VUV photons and atom bombardment. The morphology of the ice analogues is also expected to influence the scanning depth of atoms.

6.3.4 Sensitivity

The main objective of the experiment is to provide a sensitive technique to unambiguously analyze highly dilute astronomical ice analogues. The sensitivity of the instrument is tested by laser desorption of a cryogenic sample with a known isotopologue composition. We use solid Argon, which is inert and does not undergo fragmentation. The ^{36}Ar isotope has a natural abundance of 0.337 %, which we estimate to be close to the current detection threshold. Fig. 6.6 shows the laser desorption TOF mass spectrum of Ar ice at 17 K. The ^{36}Ar isotope is detected at an abundance of 0.29 % relative to the main isotope. The S/N ratio of the ^{36}Ar is 3.8 (evaluated from the values containing 95 % of the data points) setting the detection limit to ~0.3 % for molecules produced in the ices. This is better than the currently available techniques to search for species newly formed in an ice, *e.g.*, FTIR spectroscopy (1 %).

Further improvement in sensitivity can be achieved by placing the sample substrate close to the ion source in the mass spectrometer (Gudipati & Yang 2012). This minimizes dilution and allows larger portion of the desorbed species to be collected at the mass spectrometer. Reducing the dilution is particularly important for thin astronomically relevant ice samples with thickness of few hundreds of monolayers.

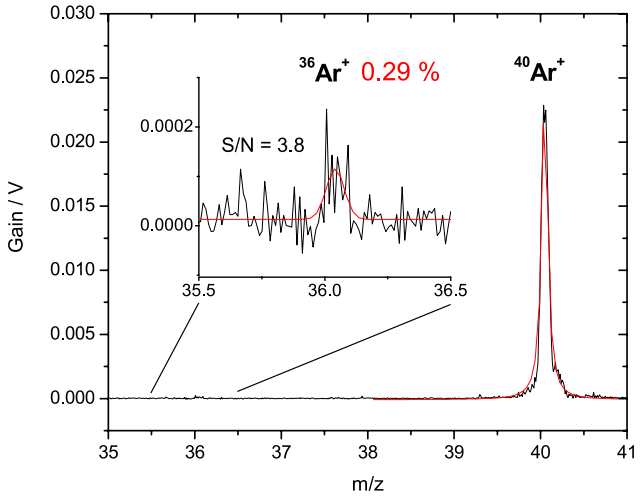

Figure 6.6 – Laser desoprtion TOF mass spectrum of solid argon at 17 K. The graph shows the m/z region with the Ar isotopologs ^{40}Ar and ^{36}Ar. The inset shows the expanded view of the ^{36}Ar peak.

6.3.5 VUV photoprocessed C_2H_6

Ethane (C_2H_6) is used as a test molecule for VUV (vacuum UV) photochemistry, due to its astronomical relevance and tendency for chemical complexation upon energetic processing. The relatively low thermal desorption temperature of 80 K makes C_2H_6 also a convenient test molecule. C_2H_2 produced through gas-phase reactions in dense cloud cores (Herbst 1995), undergoes further

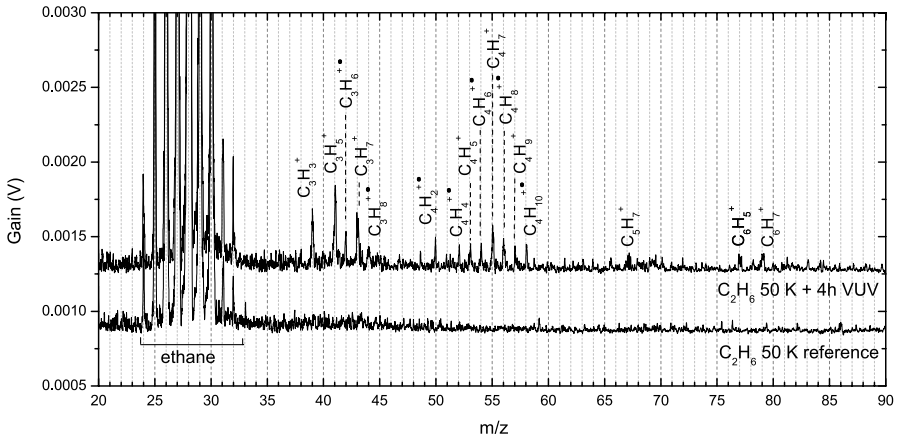

Figure 6.7 – Laser desorption TOF mass spectra of C_2H_6 at 50 K (lower trace) and after 4 h VUV photoprocessing at 50 K (upper trace). The mass signal from ethane (m/z 24–32) is saturated as a result of higher sensitivity used to see the photoproducts. The spectra are offset for clarity.

hydrogenation on grain surface yielding C_2H_6 (Charnley et al. 1995). In the laboratory C_2H_6 is readily produced through energetic processing (VUV, ion bombardment) of pure and mixed CH_4 ices (Stief et al. 1965, Gerakines et al. 1996, 2001, Kaiser & Roessler 1998, Moore & Hudson 1998, Bennett et al. 2006). Under further processing (ion/electron bombardment), C_2H_6 desaturates and polymerizes, providing a chemical route for the production ethylene (C_2H_4), acetylene (C_2H_2), methane (CH_4) as well as species with 4 carbon atoms; n-butane (C_4H_{10}) and butene (C_4H_8) (Scheer et al. 1962, Jackson et al. 1966, Strazzulla et al. 2002, Compagnini et al. 2009, Hudson et al. 2009, Kim et al. 2010).

C_2H_6 (99.99 %, Sigma Aldrich) is deposited onto a 25-mm wide substrate at 50 K. A laser desorption TOF mass spectrum of the unprocessed sample is taken for reference. A similar C_2H_6 film is deposited and subsequently exposed to VUV photons from the microwave discharge hydrogen lamp for 4 h corresponding to a dose of $\sim 7 \times 10^{17}$ photons cm^{-2}.

Fig. 6.7 shows the laser desorption TOF mass spectra of pure C_2H_6 ice before and after VUV irradiation. The heaviest mass detected for C_2H_6 corresponds to the molecular ion $C_2H_6^{+\bullet}$ at m/z 32. For VUV irradiated C_2H_6, several peaks with m/z > 32 are observed. Assuming the production of only C and H-containing photoproducts (abundance of impurities is low as deduced from the mass peaks), the detected masses between m/z 36 and 44 can be attributed to molecules containing 3 carbon atoms, and those between m/z 48 and 58 to molecules containing 4 carbon atoms. Weak signal is detected at m/z 67, 77 and 79, which suggests the presence of species with 5 and 6 carbon atoms. The m/z 77 and 79 likely corresponds to $C_6H_5^+$ and $C_6H_7^+$, respectively. The weakness and the small number of peaks, makes the detection however uncertain. These peaks may also correspond to fragments of a heavier molecular ion peak. Assuming the signal at m/z 77 and 79 corresponds to the most abundant fragments of a photoproduct with 6 carbon atoms, the fragmentation pattern points to cyclic structures; 1,3-hexadienyle and/or 1,4-hexadienyle (Fig. 6.8). Saturated aliphatic structures show maximum intensities at higher m/z values.

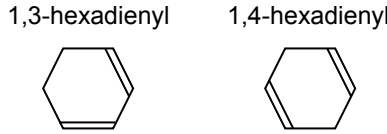

Figure 6.8 – 1,3-hexadienyl and 1,4-hexadienyl.